Indian Journal of Biochemistry & Biophysics
Vol. 63, June 2026, pp. 648-667
DOI: 10.56042/ijbb.v63i6.22453

# Unveiling anti-apoptotic mechanisms of steroidal saponins from *Dracaena draco* L. in acute myeloid leukemia cells via *in silico* modeling

Hung Duc Nguyen*, Nga Thi Thu Nguyen, Luong Trong Vu, Dung Manh Ngo & Mau Hoang Chu

Faculty of Biology, Thai Nguyen University of Education, 24000, Thai Nguyen, Vietnam

*Received 06 August 2025*; *revised 22 February 2026*

Cancer, particularly acute myeloid leukemia, remains a critical global health challenge, necessitating innovative therapeutic strategies. In Chinese traditional medicine, the resin of *Dracaena draco* L. has been used for promoting blood circulation and alleviating stasis, and steroidal saponins isolated from this plant have shown cytotoxic potential against acute myeloid leukemia cells. However, their molecular mechanisms remain insufficiently defined. Given the pivotal role of BCL-2 mediated apoptosis regulation in acute myeloid leukemia pathogenesis, this study evaluated the anti-leukemic properties of selected steroidal saponins using computational approaches. Molecular docking demonstrated CPD1's superior binding affinity (-10.93 kcal/mol) and favorable positioning within the 6GL8 binding pocket compared to venetoclax (-8.65 kcal/mol). Molecular dynamics simulations over 100 ns confirmed stable interactions underscoring CPD1's capacity to modulate BCL-2 effectively. MMGBSA analysis revealed a more favorable binding free energy for CPD1-6GL8 (-56.13 kcal/mol) than venetoclax-6GL8 (-30.29 kcal/mol). ADMET profiling indicated CPD1's non-genotoxicity, minimal hepatotoxicity, and balanced clearance, despite moderate intestinal absorption (55.034%) relative to venetoclax (100%). DFT analysis highlighted CPD1's enhanced reactivity ($\Delta E$ = 2.8949 eV) compared to venetoclax ($\Delta E$ = 4.8522 eV), reflecting greater electrophilicity (13.8734 eV *vs*. 9.0166 eV). These results position CPD1 as a promising candidate for acute myeloid leukemia therapy through BCL-2-mediated anti-apoptosis.

**Keywords**: Acute myeloid leukemia, Anti-apoptosis, DFT, *Dracaena draco* L., Molecular modeling, Steroidal saponin

Cancer constitutes a predominant global health issue, serving as a principal contributor to mortality internationally. In 2022, cancer accounted for approximately 20 million new cases and 9.7 million cancer deaths[1]. Among cancer variants, leukemia arises from chromosomal aberrations in blood progenitor cells, chiefly in bone marrow, causing an overabundance of malformed leukocytes. Leukemia's immediate dissemination, differing from the progressive expansion of solid malignancies, heightens its fatality rate. Whereas solid malignancies, including breast, prostate, or lung forms, commonly generate localized lesions before metastasis, leukemia cells circulate systemically at onset, hindering prompt diagnosis and intervention. Leukemia undergoes division into core types: acute myeloid leukemia and chronic myeloid leukemia, the latter comprising roughly 15% of adult leukemia occurrences[2]. Acute myeloid leukemia is a blood and bone marrow cancer characterized by the uncontrolled proliferation of abnormal myeloid cells, leading to a deficiency in normal blood cell production. This malignancy arises from the clonal expansion of immature myeloid precursors, disrupting normal hematopoiesis[3]. Chemotherapy remains a central and conventional approach in the management of acute myeloid leukemia. However, for older adults with acute myeloid leukemia, the five-year survival rate is indeed around 5% after diagnosis[4]. Accordingly, the continuous search for more secure and potent anti-leukemic agents is critical in advancing targeted therapies for acute myeloid leukemia.

Network pharmacology and molecular simulations represent computational methodologies utilized to explore the multi-target, multi-pathway influences of bioactive substances, particularly in leukemia management. These strategies clarify engagements between a substance and various proteins and cascades associated with leukemia progression, delivering a holistic method surpassing individual-cascade focus[5]. Implementing these strategies permits recognizing particular phytochemicals that can adjust these engagements, possibly fostering more targeted and potent leukemia interventions. Such strategies support the identification of innovative therapeutic candidates

*Correspondence:
E-mail: hungnd@tnue.edu.vn

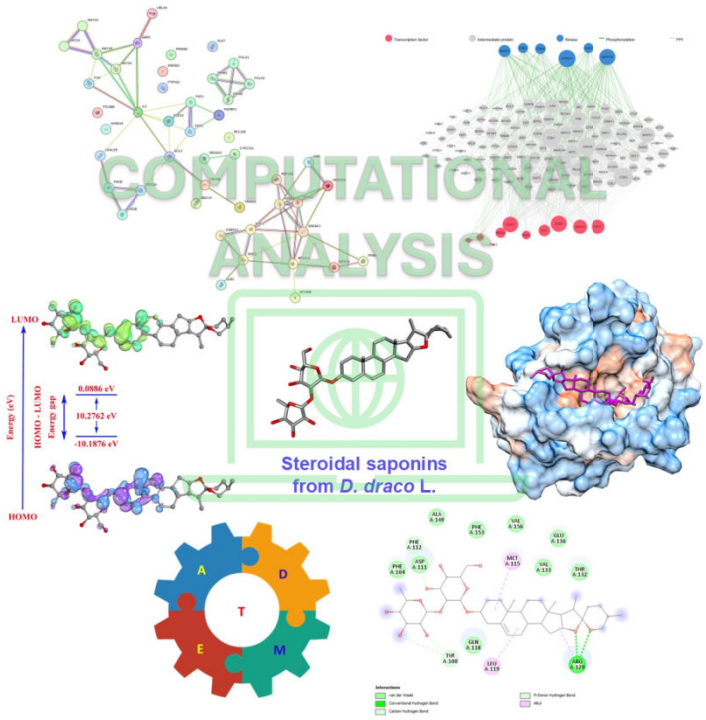


Graphical abstract

and refinement of current regimens, with advantages for patient prognosis and quality of life.

Many current cancer treatments, particularly chemotherapy drugs, are derived from plant-based compounds. These natural compounds have been a vital source of anti-cancer agents for decades, with some still in use today. Among these, steroidal saponins, a class of natural compounds, exhibit significant anti-cancer activity through various mechanisms, including inducing apoptosis and autophagy, and regulating the tumor microenvironment. They are found in many plants and have shown promise in inhibiting the proliferation of diverse cancer cell lines[6]. In Chinese traditional medicine, *Dracaena draco* L. resin, known as dragon's blood, is used for its purported ability to promote blood circulation, invigorate the blood, and alleviate blood stasis. Previous studies of our colleagues have identified steroidal saponins from this species with potential cytotoxicity against acute myeloid leukemia (HL-60 cell line)[7]. However, molecular-level details remain insufficiently explored, particularly through advanced computational tools, which prove essential to discern how natural compounds affect these targets and to provide critical insights into their mechanisms and therapeutic potential. This investigation aimed to evaluate the anti-myeloid leukemia properties of selected steroidal saponins from *D. draco* L. through a comprehensive array of computational approaches, elucidating compound-target engagements and predicting their performance. These results provide a basis for further experimental confirmation and optimization of these compounds as viable therapeutic agents for acute myeloid leukemia, subject to additional *in vitro* and *in vivo* studies.

## Experimental Section

### Preparation of selected steroidal saponins

The steroidal saponins from *D. draco* L., possessing potential cytotoxic activity against myeloid leukemia (HL-60 cell line), were selected through literature sources[7,8]. For detail, three selected steroidal steroids, including (25*R*)-spirost-5-en-3β-ol 3-*O*-{*O*-α-L-rhamnopyranosyl-(1→2)-β-D-glucopyranoside} (CPD1), Diosgenyl α-L-rhamnopyranosyl-(1→2)-[β-D-gluco-pyranosyl-(1→3)]-β-D-glucopyranoside (CPD2), 26-β-D-glucopyranosyl-22-methoxy-(25*R*)-furost-5-en-3β,26-diol-3-*O*-[α-L-rhamnopyranosyl-(1→2)][α-L-rhamnopy-ranosyl-(1→4)]-β-D-glucopyranoside (CPD3), have molecular formulas of $C_{39}H_{62}O_{12}$, $C_{45}H_{72}O_{17}$, $C_{52}H_{86}O_{22}$, and molecular weights of 722.4241, 884.4770, 1062.5611 *m/z*, respectively. Venetoclax, a

chemotherapy drug approved to treat various cancers with a molecular formula of $C_{45}H_{50}ClN_7O_7S$ and a molecular weight of 867.3181 *m/z*, was chosen as the positive control (Fig. 1).

**Molecular target prediction**

The Similarity Ensemble Approach (SEA) was employed to evaluate the two-dimensional structural similarity between each compound and ligand sets associated with specific molecular targets, quantified as an expectation value (E-value)[9]. Canonical SMILES representations of the steroidal saponins were obtained and entered into the SEA database, with *Homo sapiens* specified as the target organism to ensure predictions relevant to human biological systems. This approach facilitated the identification of biological pathways potentially regulated by these compounds, providing a foundation for subsequent mechanistic studies of their role in modulating apoptosis-driven processes in myeloid leukemia.

**Prediction of protein-protein interaction network**

To examine the protein-protein interaction (PPI) networks linked to the selected steroidal saponins, the STRING database was employed[10]. Target proteins, derived from SEA analysis, were entered into the STRING system, specifying *Homo sapiens* as the organism to ensure alignment with human physiological contexts. Such networks contribute significantly to clarifying the potential mechanisms of these compounds in a systems biology perspective.

**Biosignaling network prediction**

To explore the upstream regulatory networks linked to the target proteins of selected steroidal saponins, the X2K Web platform was employed, combining predictive data with molecular pathway analysis[11]. The X2K system integrates data on transcription factors, kinases, and protein-protein interactions to generate regulatory networks for gene sets obtained from SEA and STRING analyses, with *Homo sapiens* designated as the reference organism.

**Molecular docking**

The three-dimensional structures of selected steroidal saponins were generated in .pdb format using Biovia Discovery Studio Visualizer, including polar hydrogens and Gasteiger charge calculations, while permitting complete torsional flexibility[12]. The three-dimensional configuration of the target anti-apoptosis BCL2 (protein ID: 6GL8) was obtained in .pdb format from the RCSB Protein Data Bank[13]. Molecular docking of the protein with ligands was conducted via AutoDock Tools, employing a grid with dimensions x = 44, y = 48, z = 64, and a spacing of 0.375 Å. The docking site was defined at coordinates x = 13.009 Å, y = 1.481 Å, and z = 15.771 Å within the binding pocket of the 6GL8 protein. The Lamarckian genetic algorithm was applied to identify the most energetically favorable conformations for ligand-protein interactions.

**Molecular dynamics simulation**

Molecular dynamics simulations of the best docked pose with the 6GL8 protein were performed for 100 ns using GROMACS version 2024.4[14]. The protein structure was refined with Swiss-PdbViewer to correct for missing atoms and residues[15]. Topological parameters for the ligand were generated with SwissParam[16]. The system was solvated in a triclinic box adapted to the protein-ligand complex, employing the SPC water model and a 0.15 M concentration of

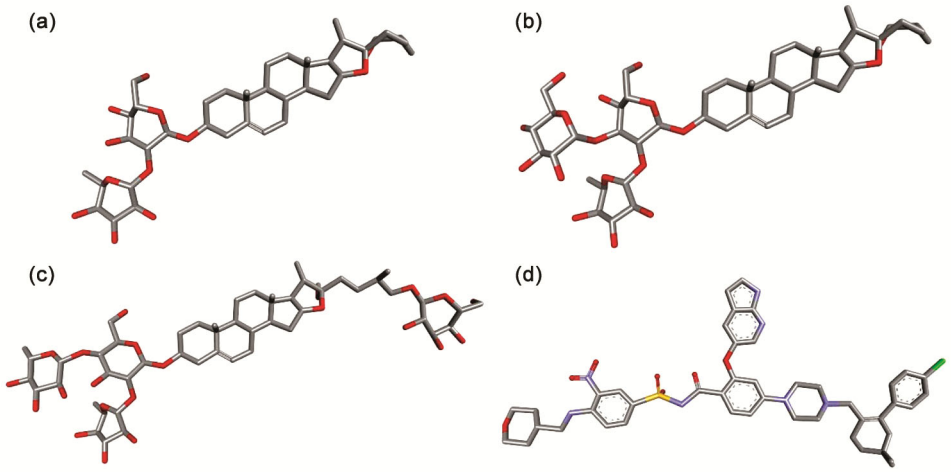


Fig. 1 — 3D Structure of the selected ligands. (a) CPD1; (b) CPD2; (c) CPD3; and (d) venetoclax

sodium chloride. Energy minimization was conducted over 50,000 steps to optimize the structure and neutralize charges. Equilibration proceeded with a 200 ps NVT ensemble (constant number of particles, volume, and temperature), succeeded by a 200 ps NPT ensemble (constant number of particles, pressure, and temperature), at 300 K and 1.0 bar. For each system, three separate 100-nanosecond simulations were run with a time step of 2 femtoseconds (0.002 ps), and trajectories were saved at 10 ns intervals. Results were analyzed with Grace software (Grace Development Team) to assess metrics such as root mean square deviation (RMSD), root mean square fluctuation (RMSF) of residues, radius of gyration (Rg), number of hydrogen bonds (Hbonds), and solvent-accessible surface area (SASA). Conformational stability of the docked ligands was evaluated by superimposition using UCSF Chimera 1.19[17]. Ligand poses at 0 ns and 100 ns were aligned to the protein binding site to examine the persistence of interactions with key amino acid residues, including hydrogen bonds, Van der Waals contacts, and hydrophobic contacts, throughout the simulation. This analysis provided insights into the dynamic behavior and binding durability of the ligand-protein complexes over 100 ns.

#### Molecular mechanics generalized born surface area (MMGBSA) analysis

The Molecular Mechanics Generalized Born Surface Area (MM/GBSA) approach represents a computational method for assessing the binding free energy of ligands to protein targets. Widely applied in drug discovery and analyses of protein-ligand associations, this method achieves an equilibrium between precision and computational demands. It integrates molecular dynamics simulations with thermodynamic evaluations to compute binding free energies. The MM/GBSA calculations, performed with gmx_MMPBSA and the charmm36-jul2022.ff force field, determined the binding free energy for the CPD1-6GL8 and venetoclax-6GL8 complexes. Electrostatic solvation energy was estimated using the Generalized Born model within a continuum solvent framework. Non-polar solvation energy was calculated based on the solvent-accessible surface area. Binding free energy values were obtained from 125 snapshots taken at intervals of 80 ps over an 80 ns molecular dynamics trajectory (from 20 ns to 100 ns). This procedure yielded an average binding energy, offering perspectives on the dynamic characteristics of protein-ligand associations and enabling assessment of binding strength and durability in a modeled setting.

#### ADMET parameters

ADMET (Absorption, Distribution, Metabolism, Excretion, and Toxicity) studies play a crucial role in elucidating the mechanism of action of natural compounds by providing insights into their pharmacokinetic properties and potential toxicity. These studies help predict how a compound will be absorbed, distributed throughout the body, metabolized, excreted, and whether it will cause adverse effects, all essential for understanding its therapeutic potential and developing it into a drug. This study analyzed the drug-likeness ADMET properties of selected compounds using the pkCSM databases[18].

#### Quantum chemistry computation using Density functional theory (DFT) method

Density Functional Theory (DFT) is increasingly applied within quantum computing frameworks to examine the characteristics of lead compounds, enabling detailed evaluation of electronic structures, molecular properties, and interaction profiles. The integration of DFT with quantum computing provides a powerful approach for predicting and analyzing the behavior of lead-based materials in diverse applications. The molecular structures of CPD1 and venetoclax were subjected to energy minimization and complete geometry optimization using the ORCA 6.1.0 software suite[19]. Input files were prepared with Avogadro software[20], and all energy calculations were conducted within the ORCA environment, with resultant data visualized and analyzed using IboView v20211019 to elucidate orbital distributions and molecular geometry[21]. DFT computations were performed at the B3LYP level of theory, utilizing the 6-31G(d,p) basis set to describe the molecular electronic wave function accurately. Molecular descriptors, including energies of the highest occupied molecular orbital (HOMO) and lowest unoccupied molecular orbital (LUMO), energy gap (ΔE), and reactivity indices such as chemical potential (μ), electronegativity (χ), hardness (η), softness (σ), and electrophilicity index (ω), were calculated based on Koopmans' theorem[22].

## Results and Discussion

#### Molecular target, protein interaction, and biosignaling network

This study initially assesses the molecular targets of selected steroidal saponins, utilizing SEA for predicting protein-ligand associations grounded in

structural similarity, STRING for mapping protein interactions to understand cellular environments, and X2K for identifying key signaling cascades that regulate apoptosis. The SEA database identified primary human molecular targets for these steroidal saponins, emphasizing IL2 (Table 1). In CPD2 and CPD3, IL2 stands out as a significant target, exhibiting p-values of 1.11E-15 and 6.07E-11, alongside MaxTC values of 0.89 and 0.61, respectively, suggesting considerable modulation of immune-related pathways that enhance caspase-3 activation, thus promoting apoptosis in malignant cells[23]. Additional key targets include ABCC4 (p-value: 1.02E-09, MaxTC: 0.28), POLA1 (p-value: 4.34E-08, MaxTC: 0.33), and CYP17A1 (p-value: 6.13E-20, MaxTC: 0.34), indicating a multifaceted

Table 1 — Molecular target prediction of selected steroidal saponins

| S. No | Compound | Target gene | Target description | *p* value | MTC |
|---|---|---|---|---|---|
| 1 | CPD1 | AMY2A | Pancreatic alpha-amylase | 1.16E-36 | 0.3 |
| | | CRYAB | Alpha-crystallin B chain | 3.67E-23 | 0.28 |
| | | DHCR24 | Delta(24)-sterol reductase | 4.75E-20 | 0.32 |
| | | CYP17A1 | Steroid 17-alpha-hydroxylase/17,20 lyase | 6.13E-20 | 0.34 |
| | | IL2 | Interleukin-2 | 6.66E-16 | 0.9 |
| | | NPC1 | NPC intracellular cholesterol transporter 1 | 8.88E-16 | 0.3 |
| | | YWHAZ | 14-3-3 protein zeta/delta | 7.88E-15 | 0.28 |
| | | ABCC4 | Multidrug resistance-associated protein 4 | 1.43E-10 | 0.31 |
| | | NPC1L1 | NPC1-like intracellular cholesterol transporter 1 | 1.19E-09 | 0.31 |
| | | FGF1 | Fibroblast growth factor 1 | 1.61E-08 | 0.28 |
| | | POLA1 | DNA polymerase alpha catalytic subunit | 1.06E-07 | 0.31 |
| | | SRD5A2 | 3-oxo-5-alpha-steroid 4-dehydrogenase 2 | 1.10E-07 | 0.32 |
| | | FGF2 | Fibroblast growth factor 2 | 5.74E-07 | 0.28 |
| | | NR1H3 | Oxysterols receptor LXR-alpha | 1.14E-06 | 0.32 |
| 2 | CPD2 | AMY2A | Pancreatic alpha-amylase | 2.57E-36 | 0.3 |
| | | CRYAB | Alpha-crystallin B chain | 6.04E-23 | 0.28 |
| | | DHCR24 | Delta(24)-sterol reductase | 7.56E-20 | 0.32 |
| | | CYP17A1 | Steroid 17-alpha-hydroxylase/17,20 lyase | 1.16E-18 | 0.33 |
| | | IL2 | Interleukin-2 | 1.11E-15 | 0.89 |
| | | NPC1 | NPC intracellular cholesterol transporter 1 | 1.22E-15 | 0.3 |
| | | ABCC4 | Multidrug resistance-associated protein 4 | 1.81E-10 | 0.31 |
| | | NPC1L1 | NPC1-like intracellular cholesterol transporter 1 | 1.44E-09 | 0.3 |
| | | POLA1 | DNA polymerase alpha catalytic subunit | 1.24E-07 | 0.3 |
| | | SRD5A2 | 3-oxo-5-alpha-steroid 4-dehydrogenase 2 | 1.30E-07 | 0.32 |
| | | EBP | 3-beta-hydroxysteroid-Delta(8),Delta(7)-isomerase | 2.64E-07 | 0.35 |
| | | NR1H3 | Oxysterols receptor LXR-alpha | 1.32E-06 | 0.32 |
| | | SREBF2 | Sterol regulatory element-binding protein 2 | 3.43E-06 | 0.28 |
| 3 | CPD3 | DHCR24 | Delta(24)-sterol reductase | 2.05E-37 | 0.32 |
| | | CRYAB | Alpha-crystallin B chain | 4.21E-24 | 0.3 |
| | | AMY2A | Pancreatic alpha-amylase | 1.42E-18 | 0.29 |
| | | NPC1L1 | NPC1-like intracellular cholesterol transporter 1 | 1.36E-17 | 0.33 |
| | | NPC1 | NPC intracellular cholesterol transporter 1 | 2.22E-16 | 0.31 |
| | | TYR | Tyrosinase | 9.17E-12 | 0.29 |
| | | IL2 | Interleukin-2 | 6.07E-11 | 0.61 |
| | | ABCC4 | Multidrug resistance-associated protein 4 | 1.02E-09 | 0.28 |
| | | NR1H3 | Oxysterols receptor LXR-alpha | 4.59E-09 | 0.33 |
| | | POLA1 | DNA polymerase alpha catalytic subunit | 4.34E-08 | 0.33 |
| | | EBP | 3-beta-hydroxysteroid-Delta(8),Delta(7)-isomerase | 6.28E-07 | 0.32 |
| | | P4HB | Protein disulfide-isomerase | 9.13E-07 | 0.3 |
| | | SREBF2 | Sterol regulatory element-binding protein 2 | 1.78E-06 | 0.3 |
| 4 | CPD4 | DHCR24 | Delta(24)-sterol reductase | 4.01E-18 | 0.29 |
| | | NPC1 | NPC intracellular cholesterol transporter 1 | 1.11E-16 | 0.32 |
| | | IL2 | Interleukin-2 | 7.60E-12 | 0.66 |
| | | ABCC4 | Multidrug resistance-associated protein 4 | 2.13E-10 | 0.3 |
| | | POLA1 | DNA polymerase alpha catalytic subunit | 7.21E-08 | 0.31 |
| | | SRD5A2 | 3-oxo-5-alpha-steroid 4-dehydrogenase 2 | 2.79E-07 | 0.34 |
| | | EBP | 3-beta-hydroxysteroid-Delta(8),Delta(7)-isomerase | 5.54E-07 | 0.33 |
| | | NPC1L1 | NPC1-like intracellular cholesterol transporter 1 | 3.29E-06 | 0.32 |

process involving disruption of multidrug resistance through ABCC4, interference with DNA replication via POLA1, and alteration of steroid production by CYP17A1[24]. Collectively, these targets support diminished cellular stress signals, a critical element in BCL2-mediated anti-apoptosis and survival promotion in myeloid leukemia cells.

Subsequent analysis with the STRING network, centered on BCL2, revealed direct connections to proteins such as IL2, FGF2, CRYAB, ERO1A, and FGF13, as illustrated in (Fig. 2). These connections highlight BCL2's participation in modulating cell survival mechanisms (through IL2 and FGF2) and adaptive responses to cellular perturbations (CRYAB and ERO1A), potentially hindering apoptosis in myeloid leukemia cells[25]. The presence of IL2 and FGF2, essential components of growth factor-mediated pathways, points to mechanisms that sustain anti-apoptotic effects via signaling cascades like MEK/ERK, thereby reinforcing BCL2 activity through transcriptional upregulation. Links to CRYAB suggest involvement in protein folding processes that may preserve BCL2 family integrity, possibly limiting the efficacy of steroidal saponins within the cellular milieu. Concurrently, alterations in IL2 activity could bolster resistance to immune surveillance, reinforcing an environment resistant to cell death. Regarding steroidal saponins engaging auxiliary proteins like SREBF2 and NR1H3, their functions in cholesterol homeostasis and gene regulation could indirectly sustain anti-apoptotic conditions by influencing membrane dynamics essential for BCL2 positioning.

Furthermore, X2K analysis produced a comprehensive network, identifying key kinases such as MAPK14, CDK1, and CSNK2A1 in (Fig. 3), which contribute to signal transduction and control of anti-apoptotic mechanisms. MAPK14 and CDK1 perform critical tasks in maintaining cellular homeostasis under stress influenced by IL2 alterations, thereby supporting BCL-2-dependent survival. At the same time, CSNK2A1 manages phosphorylation events that stabilize anti-apoptotic proteins, potentially reinforcing resistance to cell death in regulated settings

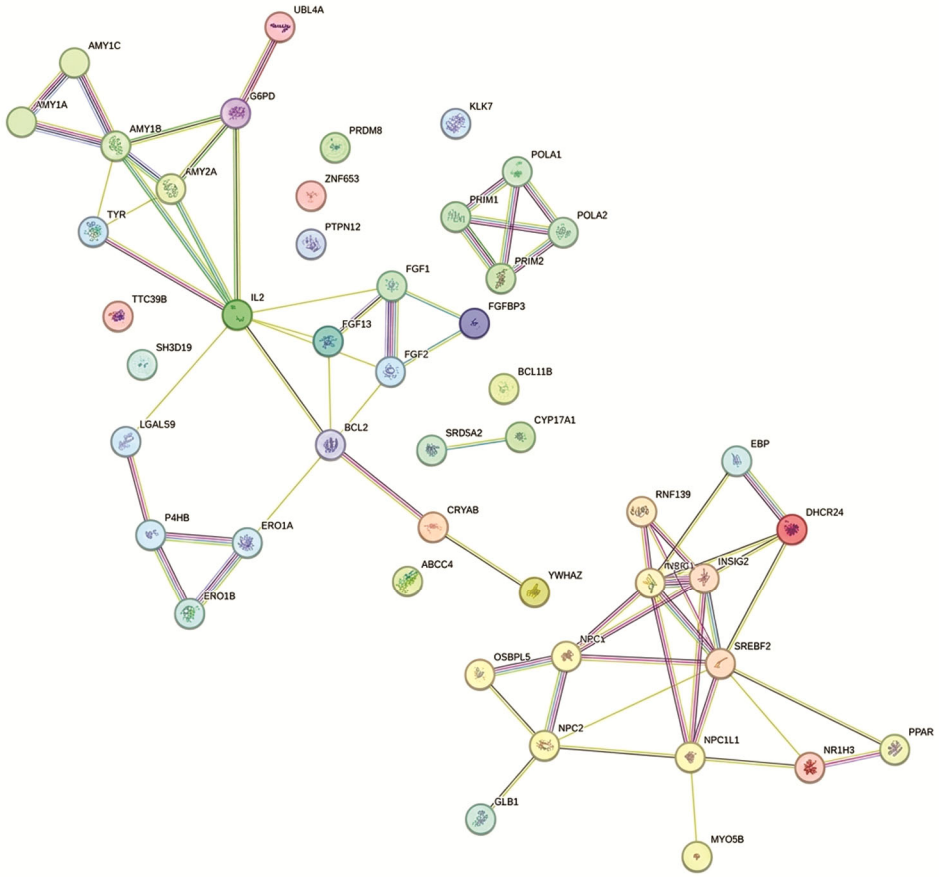


Fig. 2 — Protein-protein interactions of molecular targets of selected steroidal saponins

within myeloid leukemia[26]. X2K also extended the network to include other kinases like MAPK1 and CDK4, as shown in (Fig. 4a), which reinforce regulatory checkpoints and enzymatic cascades, leading to BCL-2 activation. Transcription factors identified in (Fig. 3) include SUZ12 (derived from epigenetic regulation targets), GATA1, and E2F1, while Figure 4b highlighted additional factors such as

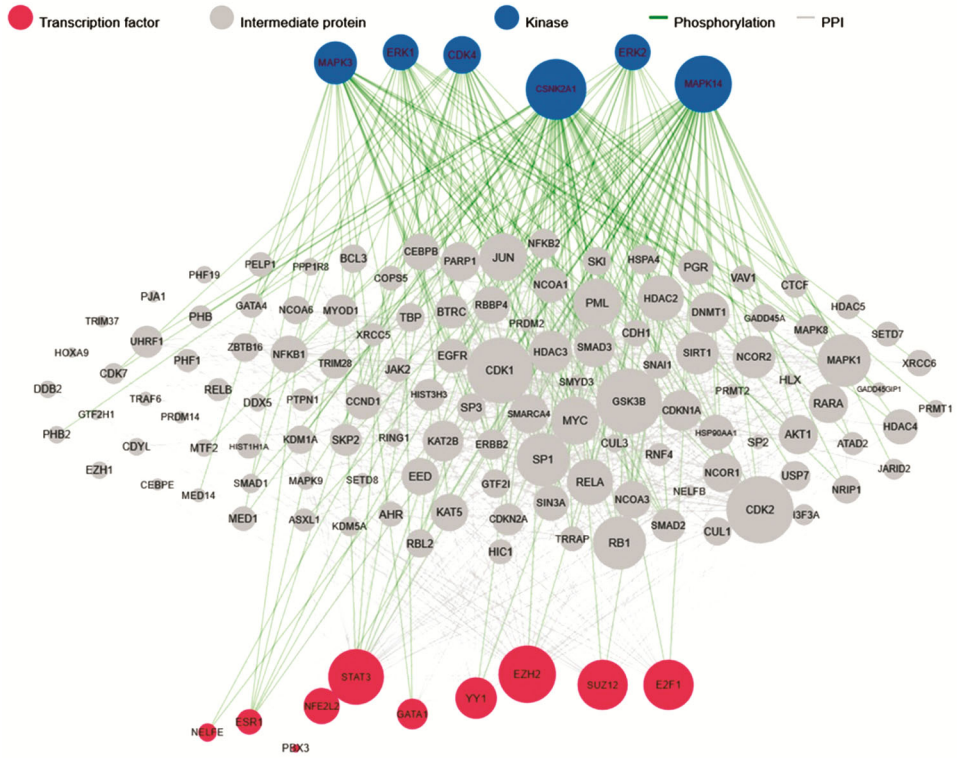


Fig. 3 — Network of kinases and transcription factors linked to molecular targets of selected steroidal saponins

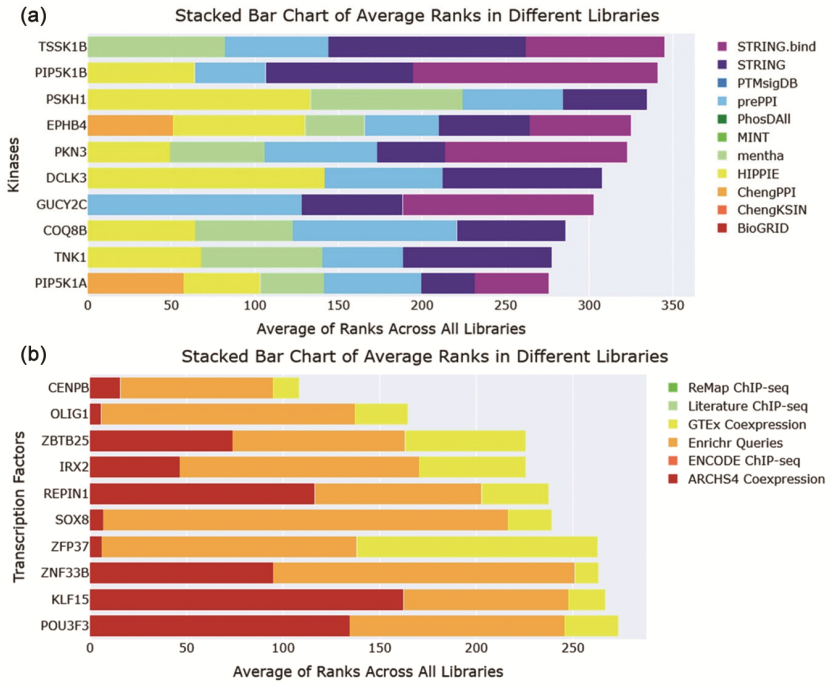


Fig. 4 — Selected steroidal saponins associated with kinases (a) and transcription factors; (b) average rank across biological libraries

ESR1. SUZ12 oversees chromatin modifications that favor survival, counteracting disturbances from IL2 imbalance, whereas GATA1 and E2F1 reduce transcription of apoptosis-promoting elements like BAX and PUMA through developmental and cell cycle pathways. ESR1 further influences hormone-responsive signaling, facilitating BCL-2 enhancement. This information supports the conclusion that selected steroidal saponins can promote anti-apoptotic conditions in myeloid leukemia via BCL-2 stabilization. The SEA analysis identified upstream targets, with IL2 as a primary focus for CPD2 and CPD3 (p-values: 1.11E-15 and 6.07E-11, MaxTC: 0.89 and 0.61), triggering survival-promoting cascades, as detailed in (Table 1); STRING mapped direct connections of BCL2 with IL2, FGF2, CRYAB, ERO1A, and FGF13, affecting these cascades, as depicted in (Fig. 2), and X2K delineated the pathways (MAPK14, CDK1, CSNK2A1, SUZ12, GATA1, E2F1) leading to anti-apoptotic gene regulation, as shown in (Figs. 3 & 4a-b).

Thus, the network evaluations suggest that these steroidal saponins enhance anti-apoptotic effects through modulation of BCL-2-mediated pathways and critical signaling networks, influencing cell viability and expansion in myeloid leukemia cells. In particular, MAPK14 coordinates stress-activated responses that bolster anti-apoptotic protein function, CDK1 governs cycle progression that favors survival when dysregulated, CSNK2A1 promotes BCL-2 stability *via* phosphorylation, SUZ12 facilitates repressive complexes linked to apoptosis evasion, and BCL-2 acts as a core regulator of mitochondrial integrity that these saponins may target for enhancement. As a result, the combined results designate BCL-2 as the chosen target for molecular docking with these steroidal saponins, potentially fostering anti-apoptotic states in myeloid leukemia cells and offering a viable approach for managing myeloid leukemia.

**Molecular docking analysis**

Molecular docking aims to computationally predict the structure and binding affinity of a ligand-receptor complex by simulating ligand interactions with a target protein's active sites. These sites, where ligands bind to form stable complexes, are critical for accurate and efficient docking predictions, enabling a targeted exploration of optimal binding poses. Accordingly, before performing ligand docking with the 6GL8 protein, the preliminary step entailed identifying active sites in the 6GL8 binding pocket. Visualization of the 6GL8 protein structure revealed residues linked to protein inhibition, including Phe104, Tyr108, Asp111, Phe112, Gln118, Leu137, Gly145, Arg146, Ala149, Phe153, and Asp171 (Fig. 5). Previous study highlighted that Tyr108, Phe112, Gln118, Leu137, and Arg146 are common key residues in the BCL-2 complexes providing valuable information for the design of potent inhibitors of BCL-2[27].

Selected steroidal saponins were evaluated through molecular docking to the 6GL8 protein, employing venetoclax as the control compound. Assessment of the docked configurations relied on their most favorable binding energy values (kcal/mol). Ligand engagements within the binding regions of the 6GL8 protein are summarized in (Table 2). Essential amino acid residues and their positions in the ligand-interaction areas were ascertained. Connections between the 6GL8 protein and chosen steroidal compounds, encompassing hydrogen bonds, Van der Waals forces, and hydrophobic interactions, are depicted in (Fig. 6).

The steroidal saponins, notably CPD1 and CPD2, exhibited distinct interaction patterns with the BCL-2 protein, a central modulator of anti-apoptosis in myeloid leukemia cells. CPD1 established 14 total interactions, including 3 hydrogen bonds (Tyr108, Asp111, Arg129), 9 Van der Waals interactions (Phe104, Phe112, Gln118, Thr132, Val133, Glu136, Ala149, Phe153, Val156), and 2 hydrophobic interactions (Met115, Leu119). Of these, residues Phe104, Tyr108, Asp111, Phe112, Gln118, Ala149,

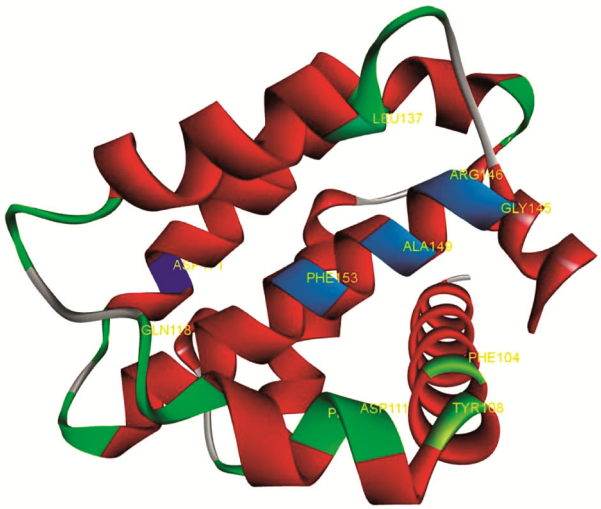


Fig. 5 — The active sites of the protein 6GL8

Table 2 — The interactions between the docked compounds and the protein 6GL8

| Docked ligands | Binding energy (kcal/mol) | Hydrogen bond interaction | Van der Waals interaction | Hydrophobic interaction |
|---|---|---|---|---|
| CPD1 | -10.93 | Tyr108, Asp111, Arg129 | Phe104, Phe112, Gln118, Thr132, Val133, Glu136, ALa149, Phe153, Val156 | Met115, Leu119 |
| CPD2 | -10.46 | Tyr108, Asp111, Arg129 | Phe104, Gln118, Thr132, Glu136, Leu137, Arg146, Ala149 | Phe112, Met115, Leu119, Val133, Phe153 |
| CPD3 | -9.91 | Glu136, Leu201, Tyr202, Gly145 | Ala100, Arg107, Asp111, Phe112, Gln118, Val133, Leu137, Asn143, Trp144, Val148, Phe153 | Phe104, Tyr108, Met115, Arg146, Ala149 |
| Venetoclax | -8.65 | Tyr108, Gly145, Arg146 | Ala100, Arg107, Asp111, Gln118, Asn143 | Phe104, Met115, Leu119, Val133, Glu136, Ley137, Arg146, Val148, Ala149, Phe153, Tyr202 |

and Phe153 occupy the active sites of the BCL-2 protein (Fig. 6a). The binding energy of CPD1 with BCL-2 reached as -10.93 kcal/mol. Likewise, CPD2 produced 15 total interactions with the BCL-2 protein, consisting of 3 hydrogen bonds (Tyr108, Asp111, Arg129), 7 Van der Waals interactions (Phe104, Gln118, Thr132, Glu136, Leu137, Arg146, Ala149), and 5 hydrophobic interactions (Phe112, Met115, Leu119, Val133, Phe153). Of these, Phe104, Tyr108, Asp111, Phe112, Gln118, Leu137, Arg146, Ala149, and Phe153 constitute amino acid residues at the active sites of the BCL-2 protein (Fig. 6b). The binding energy of CPD2 with BCL-2 registered -10.46 kcal/mol, indicating considerable durability. The binding energy of CPD3 with BCL-2 achieved -9.91 kcal/mol, signifying substantial stability. CPD3 generated 20 total interactions with the BCL-2 protein, comprising 4 hydrogen bonds (Glu136, Leu201, Tyr202, Gly145), 11 Van der Waals interactions (Ala100, Arg107, Asp111, Phe112, Gln118, Val133, Leu137, Asn143, Trp144, Val148, Phe153), and 5 hydrophobic interactions (Phe104, Tyr108, Met115, Arg146, Ala149). Among these, Phe104, Tyr108, Asp111, Phe112, Gln118, Leu137, Gly145, Arg146, Ala149, and Phe153 represent amino acid residues located at the active sites of the BCL-2 protein (Fig. 6c). The binding energy of CPD3 with BCL-2 achieved -9.91 kcal/mol, signifying substantial stability.

By contrast, venetoclax, applied as a control compound, formed 18 total interactions, with 9 directed at primary active sites (Phe104, Tyr108, Asp111, Gln118, Leu137, Gly145, Arg146, Ala149, Phe153), comprising 3 hydrogen bonds (Tyr108, Gly145, Arg146), 5 Van der Waals interactions (Ala100, Arg107, Asp111, Gln118, Asn143), and 10 hydrophobic interactions (Phe104, Met115, Leu119, Val133, Glu136, Leu137, Arg146, Val148, Ala149, Phe153, Tyr202). The binding energy of venetoclax with BCL-2 measured -8.65 kcal/mol (Fig. 6d). Despite venetoclax displaying specific engagements, its less favorable binding energy and varying interaction counts and active site participations suggest a relatively diminished interaction strength compared to three selected steroidal saponins.

Molecular docking computations of the steroidal saponins with the BCL-2 protein uncovered diverse interaction categories, such as hydrogen bonds, Van der Waals forces, and hydrophobic interactions, which collectively bolster the conformational stability of the ligand-protein entity. Hydrogen bonds constitute precise, energetically beneficial links entailing hydrogen sharing among electronegative elements like oxygen or nitrogen[28]. Hydrophobic interactions stem from the aggregation of nonpolar moieties in aqueous milieus, reducing solvent exposure and fostering their connection[29]. Although hydrogen bonds display greater potency and orientational specificity, hydrophobic interactions exert notable stabilizing effects, particularly across extensive protein-ligand interfaces. Van der Waals forces contribute significantly to fortifying protein-ligand entities during docking, permitting precise spatial arrangement between participating components and augmenting binding specificity alongside hydrogen bonding and hydrophobic effects. These noncovalent linkages remain vital for achieving a superior docking conformation. A binding energy with greater negativity typically signifies a more robust and advantageous binding event, implying superior ligand retention at the receptor[30].

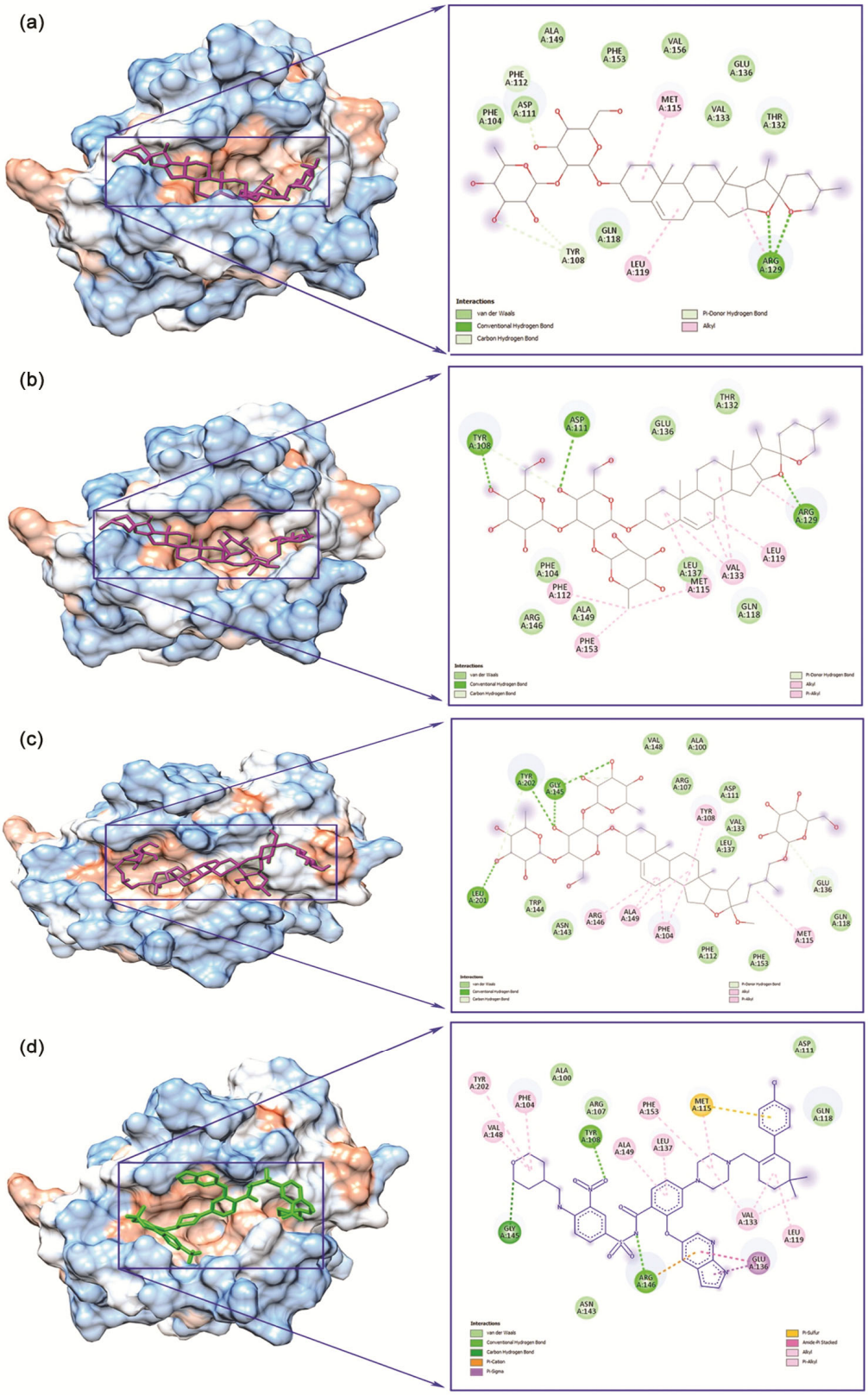


Fig. 6 — Modelling interaction diagram of docking complexes. (a) CPD1-6GL8; (b) CPD2-6GL8; (c) CPD3-6GL8; and (d) venetoclax-6GL8

The BCL-2 structure used in this work (PDB: 6GL8) corresponds to BCL-2 bound to the selective inhibitor S55746 (BCL201), which occupies the canonical BH3-binding hydrophobic groove[13]. This groove is also the pharmacological site targeted by clinically validated BH3 mimetics such as venetoclax (ABT-199)[31]. Importantly, the residues identified in our docking poses, particularly Tyr108, Asp111, Gln118, Leu137, Arg146, Gly145, Phe104, and Phe112, are consistent with residues repeatedly reported as hotspots in BCL-2 ligand recognition and stabilization of BH3-mimetic binding. In terms of docking score, venetoclax produced a binding energy of -8.65 kcal/mol, while CPD1 yielded -10.93 kcal/mol. In the literature, predicted docking free energies for venetoclax against BCL-2 vary depending on receptor form, docking engine, and scoring function. For example, docking against physiological/chimeric BCL-2 forms has reported venetoclax predicted ΔG around -10.24 to -11.35 kcal/mol, and a large-scale virtual screening study using Vina reported a venetoclax docking score of approximately -9.8 kcal/mol[32]. The somewhat less negative score observed here is therefore within the expected method-dependent range, and the more meaningful comparison becomes the conservation of key contacts within the BH3 groove rather than absolute docking energies. Notably, venetoclax pose still reproduces hallmark interactions in the 6GL8 pocket in line with reported binding-mode determinants.

Across the steroidal saponins, CPD1 and CPD2 displayed more favorable docking energies than venetoclax and engaged multiple BH3-groove hotspot residues (*e.g.*, Tyr108, Asp111, Phe112, Gln118, Leu137, Arg146). These residues were also highlighted in computational binding-mechanism analyses of BCL-2 complexes as common contributors to affinity and specificity[27]. Collectively, the alignment of CPD1's contacts with known BCL-2 hotspot residues strengthens the plausibility that CPD1 can occupy the BH3 groove in a BH3-mimetic-like manner. These results imply that CPD1, marked by the most favorable binding energy (-10.93 kcal/mol) and substantial interaction counts (14 total, with 7 at active sites), holds increased capability to inhibit BCL-2 relative to venetoclax (-8.65 kcal/mol, 18 interactions, 9 at active sites). The active sites Phe104, Tyr108, Asp111, Phe112, and Gln118, where CPD1 creates solid linkages, execute a vital function in overseeing the anti-apoptotic operation of BCL-2, as structural evidence substantiates their arrangement within the BH3-interaction cleft of the BCL-2 framework. These linkages presumably uphold the confinement of pro-apoptotic factors such as BAX and BAK, core mechanisms in anti-apoptosis governance, thereby allowing proficient alleviation of irregular apoptosis in myeloid leukemia cells. As structural reviews indicate, the invariant quality of these active sites across BCL-2 forms bolsters their relevance for extended examinations. These insights underscore the active site's role in BCL-2 inhibition, where active sites like Tyr108, Phe112 and Gln118 dominate energy contributions, making the groove an ideal target for therapeutic inhibitors[27]. This can lead to resistance, emphasizing their mechanistic importance in apoptosis regulation. Hence, CPD1 emerges as a prospective option for subsequent molecular dynamics simulations, with venetoclax functioning as a control to additionally probe the robustness and movement characteristics of the ligand-protein complex within the BCL-2 binding pocket, specifically at these vital active sites. Consistent with the docking-derived hotspot engagement, subsequent molecular dynamics simulations and MMGBSA analyses were employed to verify whether the CPD1 pose remains stable in an explicit-solvent, dynamic environment and whether the estimated binding free energy ranking persists beyond rigid-receptor docking. Notably, previous experimental studies reported that steroidal saponins from *D. draco* exert cytotoxic effects on HL-60 cells, supporting the biological relevance of this compound class[7,8]. Thus, the docking-derived BCL-2 binding model offers a target-level mechanistic hypothesis that is coherent with the reported anti-leukemic phenotype and provides a clear rationale for molecular dynamics simulations and MMGBSA validation.

**Molecular dynamics simulation**

Molecular dynamics simulations are often performed after molecular docking to validate the stability and binding poses of docked ligand-protein complexes. This helps to refine the docking results and provide a more accurate representation of how the ligand interacts with the protein in a dynamic environment. The evaluation encompassed a detailed examination of RMSD, RMSF, Rg, Hbonds, and SASA parameters to determine the conformational stability, structural variability, and surface exposure

of the CPD1-6GL8 and venetoclax-6GL8 complexes across a 100 ns simulation period. Consequently, total energy levels reached -226,358 kJ/mol for the CPD1-6GL8 complex and -228,488 kJ/mol for the venetoclax-6GL8 complex. Potential energy levels registered -281,503 kJ/mol for the CPD1-6GL8 complex and -283,584 kJ/mol for the venetoclax-6GL8 complex. Equilibrium in the simulation environment occurred at a temperature of 300 K.

The RMSD is a fundamental indicator for assessing conformational congruence among molecular structures, particularly in molecular dynamics simulations and structural comparisons. It calculates the mean separation between equivalent atoms in overlaid conformations, where a smaller RMSD signifies that the protein structures being compared are closer to each other, suggesting a higher degree of structural similarity. The RMSD trajectories for the CPD1-6GL8 and venetoclax-6GL8 complexes, observed across a 100 ns simulation interval, demonstrated comparable patterns (Fig. 7a). Both complexes displayed RMSD values ranging between 0.15 nm and 0.25 nm up to 100 ns, signifying consistent structural integrity and effective ligand attachment to the BCL-2 protein. This similarity implies that CPD1-6GL8 maintains equivalent conformational stability to venetoclax-6GL8, possibly denoting comparable binding strength at the BCL-2

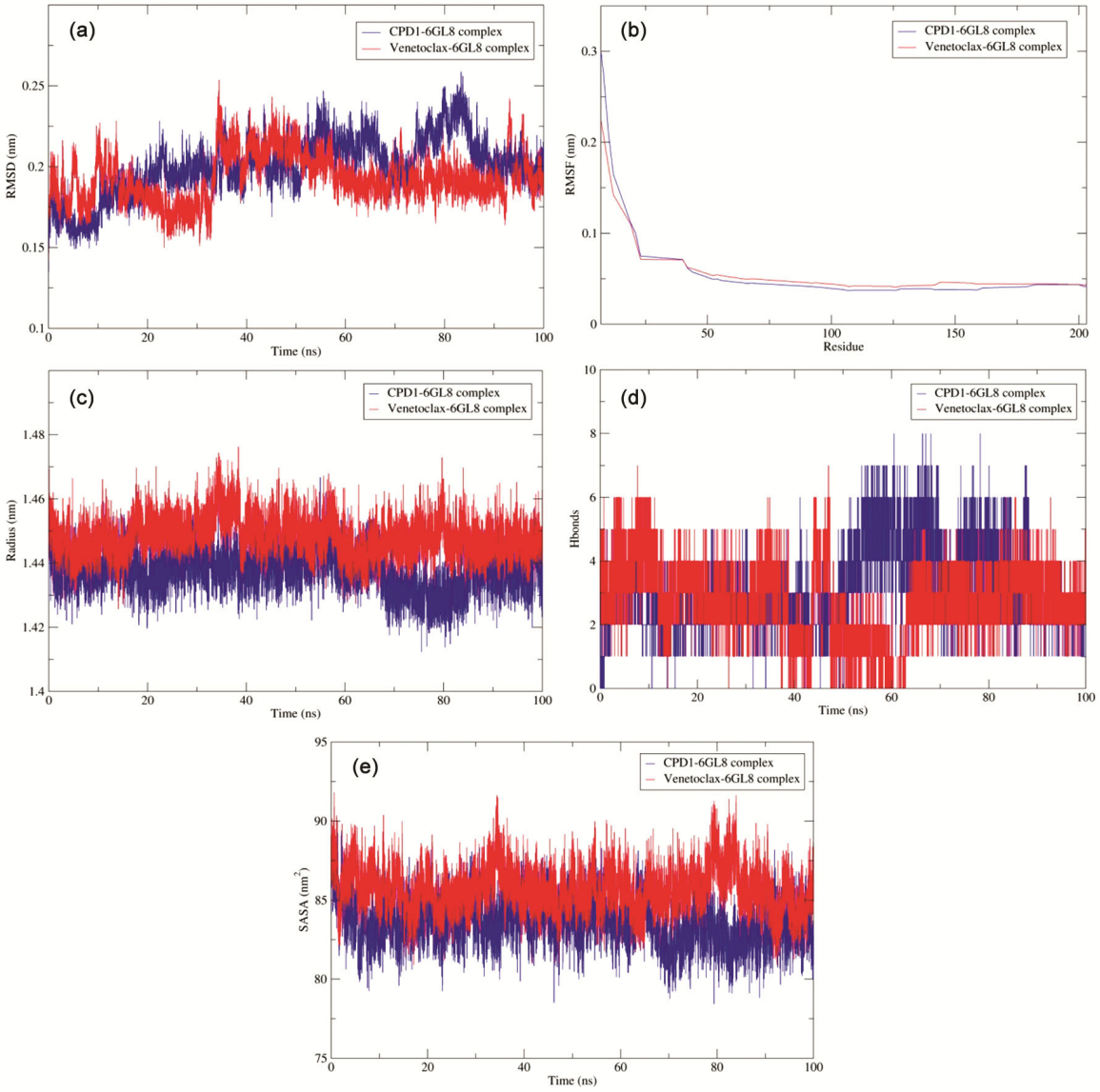


Fig. 7 — Molecular dynamics simulation results for the bindings of CPD1 (blue) and venetoclax (red) with the 6GL8 protein. (a) RMSD; (b) RMSF; (c) Rg; (d) Hbonds; and (e) SASA

active sites. Hence, the observed RMSD behaviors affirm that CPD1-6GL8 preserves its baseline configuration more reliably than the venetoclax-6GL8 complex.

The RMSF measures how much individual parts of a protein move relative to their average position, highlighting flexible regions. The RMSF trajectories for the CPD1-6GL8 and venetoclax-6GL8 complexes were analyzed over a 100 ns simulation duration, with variability observed from residues Gly7 to Gly203. This fluctuation likely stems from the comparative positioning of these residues relative to critical active binding locations, such as sites involving Phe104 and Tyr108. The CPD1-6GL8 complex demonstrates RMSF values varying at an average of 0.3 to 0.05 nm, indicating a shift toward consistent architectural firmness. Similarly, the venetoclax-6GL8 complex presents RMSF declining from 0.22 nm at Gly7 to 0.05 nm at Gly203, reflecting an analogous consolidation trend (Fig. 7b). In comparison, the venetoclax-6GL8 complex reveals a somewhat elevated starting variability. This arrangement proposes that CPD1-6GL8 undergoes a more tempered structural adjustment relative to venetoclax-6GL8. Therefore, the CPD1-6GL8 complex attains superior architectural uniformity with reduced variability past residue Gly7, emphasizing its capacity to manage molecular engagements within the BCL-2 protein active domain proficiently.

The Rg evaluates the compactness of a protein by computing the root mean square distance of all atoms from the protein's mass center, thus acting as an index of its spatial organization. A smaller Rg in a protein structure generally indicates a more compact and globular shape, while a larger Rg value is associated with a more extended and flexible structure[33]. The analysis of Rg values for the complexes is shown in (Fig. 7c). The Rg values for the CPD1-6GL8 and venetoclax-6GL8 complexes manifested differing oscillations between 1.42 and 1.48 nm, with an approximate average of 1.44 nm throughout the 100 ns simulation period, intimating that both complexes retain a reliably dense arrangement of the BCL-2 protein during the simulation.

The Hbonds play a crucial role in molecular dynamics simulations, significantly influencing structural stability, flexibility, and how molecules interact[34]. The occurrence of hydrogen bonds persisted throughout the simulation, with the CPD1-6GL8 complex exhibiting a range of 1 to 8 bonds and the venetoclax-6GL8 complex showing 1 to 7 bonds. These results suggest that both complexes maintain stable interactions within the BCL-2 protein binding site throughout the simulation, with the CPD1-6GL8 complex exhibiting a slightly greater number of hydrogen bonds than the venetoclax-6GL8 complex (Fig. 7d). This difference indicates that CPD1 forms a broader network of interactions with the BCL-2 protein.

Solvent-accessible surface area (SASA) quantifies the area of a molecule's surface accessible to solvent molecules, often modeled as spheres. This metric is crucial in understanding molecular interactions, particularly in biological systems, including protein folding, ligand binding, and overall molecular dynamics[35]. The SASA profiles of the CPD1-6GL8 and venetoclax-6GL8 complexes were analyzed to assess their solvent exposure properties. Over the 100 ns simulation period, the SASA trajectory revealed dynamic changes, with the CPD1-6GL8 complex fluctuating between 80 and 87 $nm^2$ and the venetoclax-6GL8 complex ranging from 82.5 to 92.5 $nm^2$ (Fig. 7e). These fluctuations likely reflect ligand-induced changes in solvent accessibility, indicating adjustments at the BCL-2-ligand interface that may affect binding characteristics. The similar range and average SASA values for both complexes suggest consistent maintenance of their solvent-exposed surfaces, despite CPD1's more favorable docking binding energy (-10.93 kcal/mol) compared to venetoclax (-8.65 kcal/mol), hinting at potential differences in binding interactions.

The detailed analysis of dynamic parameters has provided clear insights into the stability and structural characteristics of the CPD1-6GL8 and venetoclax-6GL8 complexes, highlighting the BCL-2 protein's role in molecular interactions. The study showed that the CPD1-6GL8 complex exhibits comparable stability to the venetoclax-6GL8 complex in its interaction with the BCL-2 protein, positioning CPD1 as a promising candidate. These findings, consistent with CPD1's more favorable docking binding energy (-10.93 kcal/mol) compared to venetoclax (-8.65 kcal/mol), emphasize its ability to maintain strong binding to the BCL-2 protein. The 100 ns molecular dynamics simulations trajectories showed that both CPD1-6GL8 and venetoclax-6GL8 complexes remained structurally stable (protein backbone RMSD of 0.15-0.25 nm), with persistent hydrogen-bonding and compactness (Rg of 1.42-1.48 nm). Similar

RMSD magnitudes have been reported in molecular dynamics simulations studies of BCL-2 complexes with venetoclax and other ligands, supporting that RMSD values in this range generally reflect a well-equilibrated complex without major unfolding or pocket disruption.

**Free binding energy (MMGBSA) analysis**

The binding free energies of ligand-protein complexes underwent computation using the MM/GBSA approach, executed through gmx_MMPBSA software with the charmm36-jul2022.ff force field. The Molecular Mechanics/Generalized Born Surface Area (MM-GBSA) examination utilized 100 ns molecular dynamics simulation trajectories. The binding free energy (ΔG_binding) for ligand-protein systems is formulated as ΔG_binding = G_complex - (G_receptor + G_ligand), where G_receptor represents the free receptor energy and G_ligand the free ligand energy. Alternatively, ΔG_binding approximates ΔH - TΔS, with ΔH as binding enthalpy and -TΔS as entropy shift from binding-induced conformational changes. Without explicit entropy calculations, the derived value is an approximate effective free energy for relative binding strength comparisons in analogous setups. This investigation calculated the effective free energy over 100 ns, employing 125 frames sampled at 80 ps intervals from 0 to 100 ns. This methodology yielded an average binding energy, depicting the kinetic features of protein-ligand engagements and providing perspectives on affinity and durability under modeled scenarios. As detailed in (Table 3), MMGBSA computations for CPD1-6GL8 and venetoclax-6GL8 complexes yielded average binding free energies (ΔTOTAL) of -56.13 kcal/mol for CPD1-6GL8 and -30.29 kcal/mol for venetoclax-6GL8. Contributing factors to ΔTOTAL encompass van der Waals forces (ΔVDWAALS) at -51.30 kcal/mol for CPD1-6GL8 and -53.11 kcal/mol for venetoclax-6GL8, electrostatic forces (ΔEEL) at -46.12 kcal/mol and 41.63 kcal/mol, respectively, and solvation terms (ΔGSOLV) at 41.29 kcal/mol for CPD1-6GL8 and -18.81 kcal/mol for venetoclax-6GL8. Terms like bond, angle, dihedral, and 1-4 interactions contributed minimally (0.00 kcal/mol or near zero). The substantially more negative ΔTOTAL for CPD1-6GL8 implies greater binding strength and improved stability relative to venetoclax-6GL8, largely attributed to advantageous van der Waals and electrostatic contributions, offsetting a positive solvation cost.

***In silico* ADMET characteristics**

In this study, ADMET evaluations were performed utilizing the pkCSM platform to determine the oral bioavailability of CPD1 and venetoclax, with results summarized in (Table 4). Absorption in ADMET prediction represents how a drug enters the bloodstream and becomes available to reach its target site. Understanding and accurately predicting a drug's absorption is essential for determining its efficacy and safety. The data revealed that CPD1 and venetoclax exhibit differing absorption characteristics. Water solubility proved superior for venetoclax (-3.037 log mol/L) compared to CPD1 (-4.279). Caco2 permeability appeared higher for venetoclax (0.847

Table 3 — Free energy of binding obtained using MMGBSA calculations

| Energy Component | Average (kcal/mol) | | Standard Deviation | |
|---|---|---|---|---|
| | CPD1-6GL8 | Venetoclax-6GL8 | CPD1-6GL8 | Venetoclax-6GL8 |
| ΔBOND | 0.00 | 0.00 | 0.00 | 0.00 |
| ΔANGLE | -0.00 | -0.00 | 0.00 | 0.00 |
| ΔDIHED | 0.00 | -0.00 | 0.00 | 0.00 |
| ΔUB | 0.00 | 0.00 | 0.00 | 0.00 |
| ΔIMP | -0.00 | -0.00 | 0.00 | 0.00 |
| ΔCMAP | 0.00 | 0.00 | 0.00 | 0.00 |
| ΔVDWAΔALS | -51.30 | -53.11 | 5.16 | 7.12 |
| ΔEEL | -46.12 | 41.63 | 17.72 | 30.05 |
| Δ1-4 VDW | 0.00 | -0.00 | 0.00 | 0.00 |
| Δ1-4 EEL | 0.00 | -0.00 | 0.00 | 0.00 |
| ΔEGB | 48.46 | -11.28 | 14.34 | 26.53 |
| ΔESURF | -7.17 | -7.53 | 0.80 | 0.69 |
| ΔGGAS | -97.42 | -11.48 | 19.62 | 30.36 |
| ΔGSOLV | 41.29 | -18.81 | 13.72 | 26.39 |
| ΔTOTAL | -56.13 | -30.29 | 7.65 | 6.92 |

Table 4 — Predicted properties ADMET of CPD1 and venetoclax

| ADMET properties | Unit | CPD1 | Venetoclax |
|---|---|---|---|
| Water Solubility | (Log mol/L) | -4.279 | -3.037 |
| Caco2 permeability | (Log Papp in 10-6 cm/s) | 0.34 | 0.847 |
| Intestinal absorption (Human) | (% Absorbed) | 55.034 | 100 |
| Skin permeability | (Log Kp) | -2.738 | -2.735 |
| P-glycoprotein substrate | Yes/No | Yes | Yes |
| P-glycoprotein I inhibitor | Yes/No | Yes | Yes |
| P-glycoprotein II inhibitor | Yes/No | No | Yes |
| VDss | (Log L/kg) | -0.385 | -0.329 |
| Fraction unbound (human) | (Fu) | 0.315 | 0.169 |
| BBB permeability | (Log BB) | -1.706 | -1.747 |
| CNS permeability | (Log PS) | -3.896 | -3.119 |
| CYP2D6 substrate | Yes/No | No | No |
| CYP3A4 substrate | Yes/No | Yes | Yes |
| CYP1A2 inhibitor | Yes/No | No | No |
| CYP2C19 inhibitor | Yes/No | No | No |
| CYP2C9 inhibitor | Yes/No | No | No |
| CYP2D6 inhibitor | Yes/No | No | No |
| CYP3A4 inhibitor | Yes/No | No | Yes |
| Total clearance | (Log ml/min/kg) | 0.359 | -0.096 |
| Renal OCT2 substrate | Yes/No | No | No |
| AMES toxicity | Yes/No | No | No |
| Max. tolerated dose (human) | (Log mg/kg/day) | -2.086 | 0.278 |
| hERG I inhibitor | Yes/No | No | No |
| hERG II inhibitor | Yes/No | Yes | Yes |
| Oral rat acute toxicity (LD50) | (mol/kg) | 4.164 | 2.604 |
| Oral rat chronic toxicity (LOAEL) | (Log mg/kg_bw/day) | 3.334 | 1.924 |
| Hepatotoxicity | Yes/No | No | Yes |
| Skin sensation | Yes/No | No | No |
| *Tetrahymena pyriformis* toxicity | (Log ug/L) | 0.285 | 0.285 |
| Minnow toxicity | (Log mM) | 3.223 | -0.481 |

log Papp in $10^{-6}$ cm/s) than CPD1 (0.34). Intestinal absorption reached 100% for venetoclax, exceeding CPD1 (55.034%). Skin permeability remained comparable between CPD1 (-2.738 log Kp) and venetoclax (-2.735). Both compounds act as P-glycoprotein substrates and inhibit P-glycoprotein I, though venetoclax additionally inhibits P-glycoprotein II, potentially influencing efflux dynamics. Overall, venetoclax demonstrates enhanced absorption, whereas CPD1's profile suggests moderate bioavailability, possibly necessitating formulation adjustments for improved efficacy.

Predicting drug distribution is crucial for optimizing drug efficacy and minimizing potential side effects. Understanding how a drug distributes throughout the body determines its concentration at the target site, which directly impacts its therapeutic effect[36]. Drug distribution receives assessment via steady-state volume of distribution (VDss), reflecting dispersal from plasma to tissues; values exceeding 0.45 log L/kg denote high tissue uptake. Table 4 indicates venetoclax exhibits marginally higher tissue distribution (-0.329 log L/kg) than CPD1 (-0.385), both suggesting limited penetration. The unbound fraction (Fu) in plasma stands at 0.315 for CPD1 and 0.169 for venetoclax, implying CPD1 offers greater free drug availability. For blood-brain barrier (BBB) permeability, log BB >0.3 indicates strong crossing, while <-1 signals weak; both CPD1 (-1.706) and venetoclax (-1.747) show poor BBB access. CNS permeability follows log PS >-2 for entry and <-3 for exclusion[37]; CPD1 (-3.896) lacks CNS access,

whereas venetoclax (-3.119) borders on limited entry. CPD1 presents a favorable unbound fraction but restricted CNS distribution, potentially limiting central effects, while venetoclax balances modest tissue spread with a slight CNS advantage. However, formulation may enhance CPD1's profile for BCL-2 inhibition in myeloid leukemia.

Drug metabolism is a crucial process that significantly affects how a drug behaves in the body. It influences how the body processes the drug, its effects, and its safety profile. CYP450 enzymes are crucial for metabolizing most drugs used in clinical practice, with CYP3A4 and CYP2D6 being the most significant. Other drugs can inhibit or induce these enzymes, potentially leading to drug interactions and unexpected reactions[38]. CPD1 and venetoclax serve as substrates for CYP3A4, signifying metabolism via this pathway, which is common among pharmaceuticals, but neither acts as a substrate for CYP2D6. Regarding inhibition, neither CPD1 nor venetoclax affects CYP1A2, CYP2C19, CYP2C9, or CYP2D6. Venetoclax inhibits CYP3A4, whereas CPD1 does not, implying reduced potential for interactions involving this enzyme in CPD1. Considering the emphasis on myeloid leukemia therapy, where limiting metabolic conflicts proves important, CPD1 emerges as the favorable option. Its lack of CYP3A4 inhibition may yield a safer metabolic pattern than venetoclax, which could elevate drug levels and risks, though both share CYP3A4 substrate status.

Excretion assessment, a key component of ADMET profiling, elucidates the elimination dynamics of compounds from the body. Total clearance, expressed in log mL/min/kg, quantifies the rate of compound removal. CPD1 demonstrates a clearance rate of 0.359 log mL/min/kg, while venetoclax exhibits a negative value of -0.096 log ml/min/kg, indicating slower elimination and potential retention. Neither compound serves as a substrate for renal OCT2, suggesting excretion independent of this transporter. For myeloid leukemia therapy targeting BCL-2 inhibition, CPD1's moderate clearance rate offers a balanced profile, facilitating effective elimination while minimizing accumulation risks compared to venetoclax's slower clearance, which may prolong systemic exposure.

ADMET toxicity evaluation aims to predict and understand how a drug candidate will behave in the body, including its potential to cause adverse effects. CPD1's maximum tolerated dose (-2.086 log mg/kg/day) indicates lower tolerability than venetoclax (0.278 log mg/kg/day). Neither inhibits hERG I, but both inhibit hERG II, suggesting cardiac channel interactions. Acute oral rat toxicity (LD50) revealed CPD1 (4.164 mol/kg) as less toxic than venetoclax (2.604 mol/kg); chronic toxicity (LOAEL) showed CPD1 (3.334 log mg/kg_bw/day) with lower toxicity than venetoclax (1.924 log mg/kg_bw/day). Venetoclax exhibits hepatotoxicity, unlike CPD1. Both lack skin sensitization. T. Pyriformis toxicity was identical (0.285 log ug/L), but CPD1 had higher minnow toxicity (3.223 log mM) versus venetoclax (-0.481 log mM). For BCL-2 inhibition in myeloid leukemia, CPD1's safer profile, with no hepatotoxicity and lower chronic toxicity, supports its selection for dynamics simulations over venetoclax, despite reduced tolerability.

The *in silico* ADMET analysis of CPD1 and venetoclax indicates that CPD1 satisfies key pharmacokinetic requirements, including lack of genotoxicity, lower hepatotoxicity, and intermediate clearance kinetics. Thus, CPD1 is a viable therapeutic option for myeloid leukemia, enhancing apoptosis via BCL-2 (6GL8) inhibition. Additionally, CPD1 offers a foundation for synthesizing new derivatives with superior efficacy, favorable safety attributes, and expanded applications in cancer treatment.

**Quantum chemistry computation using DFT method**

DFT is a computational method used in Computer-Aided Drug Design to analyze the electronic structure and properties of molecules, aiding in predicting their behavior and interactions. By calculating properties like binding affinity, electronic structure, and reactivity, DFT helps identify promising drug candidates and optimize their design[39]. This study performed DFT computations with ORCA 6.1.0 and IboView v20211019. Density functional theory assessments were applied to CPD1 and venetoclax to explore their binding capabilities with the target protein, producing varied outcomes as summarized in (Table 5). The highest occupied molecular orbital

Table 5 — Quantum descriptors of CPD1 and venetoclax

| Molecule | EHOMO (eV) | ELUMO (eV) | ΔE (eV) | μ (eV) | χ (eV) | η (eV) | σ ($eV^{-1}$) | ω (eV) |
|---|---|---|---|---|---|---|---|---|
| CPD1 | -7.7848 | -4.8899 | 2.8949 | -6.3374 | 6.3374 | 1.4475 | 0.6909 | 13.8734 |
| Venetoclax | -9.0405 | -4.1883 | 4.8522 | -6.6144 | 6.6144 | 2.4261 | 0.4122 | 9.0166 |

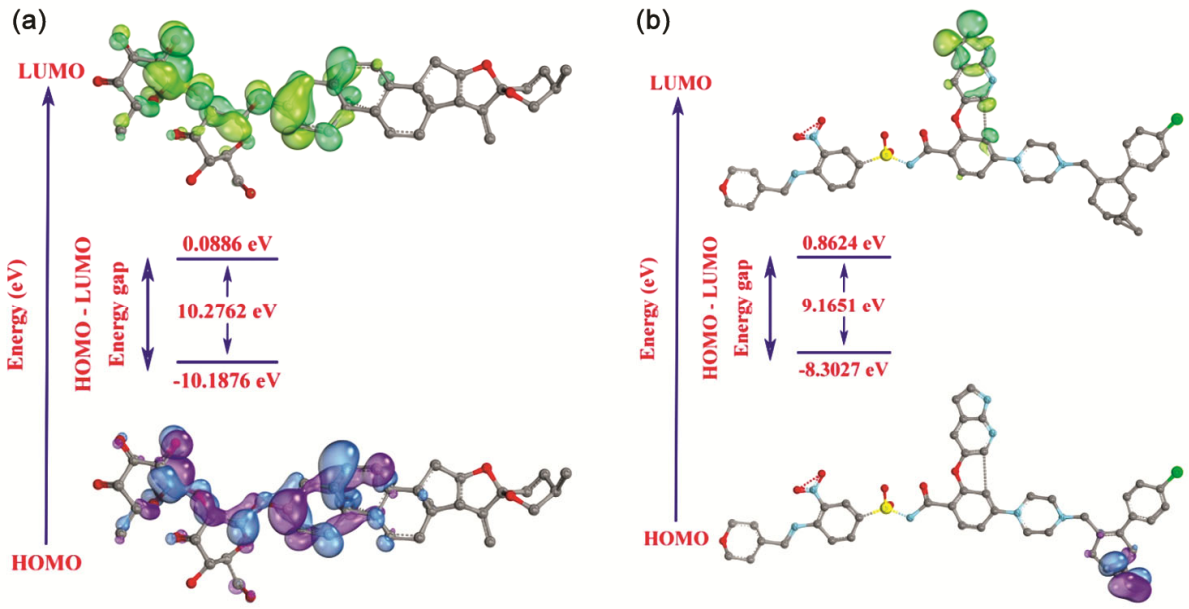


Fig. 8 — HOMO and LUMO surface diagrams of (a) CPD1; and (b) venetoclax

(HOMO) and lowest unoccupied molecular orbital (LUMO) energies offer vital information regarding molecular traits, kinetic behavior, and engagement patterns of these substances, as illustrated in (Fig. 8). The HOMO energy signifies electron-donating potential. In contrast, the LUMO energy reflects electron-accepting capacity. CPD1 exhibits a higher EHOMO (-7.7848 eV) relative to venetoclax (-9.0405 eV), implying increased electron-donating tendency and greater vulnerability to oxidation. In contrast, CPD1 possesses a lower LUMO energy (-4.8899 eV) than venetoclax (-4.1883 eV), denoting stronger electron-accepting propensity. The energy difference (ΔE) acts as an index for gauging durability and chemical kinetics, where a smaller difference generally signals elevated kinetics and lesser durability, and a larger difference conveys superior durability and limited kinetics[40]. CPD1 features a ΔE of 2.8949 eV, whereas venetoclax features a ΔE of 4.8522 eV, inferring that CPD1 displays marginally elevated kinetics and lesser durability than venetoclax. Ionization potential (IP), equated to the negative HOMO energy, quantifies the energy for electron detachment, with elevated figures indicating heightened resilience against oxidation. Electron affinity (EA), estimated as the negative LUMO energy, appraises a system's electron-acquisition aptitude. Greater EA values (more negative LUMO energies) denote pronounced electron-attraction tendencies, signaling advanced electron-receptor qualities[41]. CPD1 registers an IP of 7.7848 eV and an EA of 4.8899 eV, while venetoclax records an IP of 9.0405 eV and an EA of 4.1883 eV, underscoring CPD1's enhanced electron-attraction dominance. Chemical hardness (η), derived as half the energy difference ($\eta = \Delta E/2$), evaluates opposition to electron cloud distortions, whereas softness (σ), the reciprocal of hardness ($\sigma = 1/\eta$), reflects susceptibility to kinetic processes[42]. CPD1 manifests a hardness of 1.4475 eV and a softness of 0.6909 $eV^{-1}$, against venetoclax's hardness of 2.4261 eV and softness of 0.4122 $eV^{-1}$, intimating CPD1 exhibits somewhat greater kinetic predisposition. Electronegativity (χ), computed as the mean of IP and EA ($\chi = (IP + EA)/2$), gauges the power to pull electron clouds. CPD1 attains a χ of 6.3374 eV, and venetoclax a χ of 6.6144 eV, revealing venetoclax's marginally stronger electron-pulling inclination. Chemical potential (μ), the negative electronegativity ($\mu = -\chi$), describes a system's propensity to gain or lose electrons. More negative chemical potential figures indicate a pronounced inclination toward electron gain[43]. CPD1 presents a μ of -6.3374 eV, and venetoclax a μ of -6.6144 eV, consistent with venetoclax's superior electron-gain preference. The electrophilicity index (ω), formulated as $\omega = \mu^2/(2\eta)$, measures electrophilic potency, with higher figures signifying more evident electrophilic traits[44]. CPD1 logs an ω of 13.8734 eV, while venetoclax logs 9.0166 eV, proposing CPD1's amplified aptitude for electrophilic engagements with physiological targets.

Frontier molecular orbital (FMO) descriptors (HOMO/LUMO and ΔE) are commonly used to rationalize chemical reactivity and propensity for charge transfer, where a smaller HOMO-LUMO gap is often associated with higher polarizability and reactivity, which can facilitate noncovalent recognition processes in biological environments. In this work, CPD1 exhibits a smaller ΔE than venetoclax, suggesting a comparatively higher electronic flexibility. This interpretation is consistent with the frequently reported view that reduced ΔE may support stronger intermolecular interactions via easier electronic redistribution upon binding. In addition, CPD1 shows a higher electrophilicity index (ω) than venetoclax under the same computational level, implying an enhanced tendency to accept electron density from electron-rich environments. Such a profile can be compatible with the BH3-groove binding context, where a ligand simultaneously experiences hydrophobic packing and localized polar/charged anchors (*e.g*., Tyr108, Asp111, Arg146)[45]. Therefore, the DFT results provide an electronic-structure rationale that complements docking/MD observations: CPD1's predicted electronic adaptability may help sustain its multi-contact interaction network within the BCL-2 groove.

## Conclusion

The pharmacodynamics and binding targets of steroidal saponins from *D. draco* L. as potential anti-apoptotic agents in myeloid leukemia. The findings demonstrated that these saponins likely promote cell survival through regulation of critical pathways, with IL2 modulation reducing oxidative stress and inhibiting pro-apoptotic factors, while influencing viability via targets like DHCR24 and CRYAB. Molecular docking studies with the protein 6GL8 showed that CPD1 achieves greater stability and optimal positioning within the 6GL8 binding pocket compared to venetoclax. The molecular dynamics simulation substantiated a reliable engagement pattern, with consistent associations preserved over 100 ns, as indicated by RMSD ranges of 0.15-0.25 nm, Rg values of 1.42-1.44 nm, and fluctuating hydrogen bond formations, emphasizing CPD1's capacity to modulate 6GL8 effectively. MMGBSA computations yielded a more favorable binding free energy for CPD1-6GL8 (-56.13 kcal/mol) relative to venetoclax-6GL8 (-30.29 kcal/mol), bolstered by advantageous van der Waals and electrostatic terms offsetting solvation penalties, reflecting superior potency. DFT examination disclosed differing kinetic profiles, with CPD1 featuring elevated HOMO energy (-7.7848 eV) and a narrowed energy gap (2.8949 eV) versus venetoclax (-9.0405 eV and 4.8522 eV), denoting heightened electron-donation, kinetics, and electrophilicity (13.8734 eV vs. 9.0166 eV). From the *in silico* ADMET profiling outcomes for CPD1 and venetoclax, CPD1 fulfills fundamental pharmacokinetic benchmarks, showing absence of genotoxicity, minimal hepatotoxicity, and balanced clearance. Accordingly, CPD1 emerges as a prospective therapeutic for myeloid leukemia by enhancing anti-apoptosis via BCL-2 (6GL8) modulation. Furthermore, CPD1 may provide a platform for synthesizing advanced derivatives with augmented potency, refined safety, and broadened roles in neoplasm management.

## Conflict of interest

All authors declare no conflicts of interest.

## References

1 Bray F, Laversanne M, Sung H, Ferlay J, Siegel RL, Soerjomataram I & Jemal A, Global cancer statistics 2022: GLOBOCAN estimates of incidence and mortality worldwide for 36 cancers in 185 countries. *CA Cancer J Clin*, 74 (2024) 229.

2 Makkar H, Majhi RK, Goel H, Gupta AK, Chopra A, Tanwar P & Seth R, Acute myeloid leukemia: novel mutations and their clinical implications. *Am J Blood Res*, 13 (2023) 12.

3 Wang M, Wang Y, Chen L, Yu S, Li X, Huang G & Jin M, Baicalein suppresses the malignant progression of acute myeloid leukemia *via* ROS-dependent metabolic reprogramming: Mechanisms of differentiation induction and ferroptosis activation. *Eur J Pharmacol*, 1002 (2025) 177839.

4 Button E, Carter H, Gavin NC, LeBlanc TW & McCaffrey N, A systematic review of health state utility values for older people with acute myeloid leukaemia. *Qual Life Res*, 33 (2024) 2899.

5 Hong J, Liu W, Xiao X, Gajendran B & Ben-David Y, Targeting pivotal amino acids metabolism for treatment of leukemia. *Heliyon*, 10 (2024) e40492.

6 Bouabdallah S, Al-Maktoum A & Amin A, Steroidal saponins: Naturally occurring compounds as inhibitors of the hallmarks of cancer. *Cancers*, 15 (2023) 3900.

7 Mimaki Y, Kuroda M, Ide A, Kameyama A, Yokosuka A & Sashida Y, Steroidal saponins from the aerial parts of Dracaena draco and their cytostatic activity on HL-60 cells. *Phytochemistry*, 50 (1999) 805.

8 González AG, Hernández JC, León F, Padrón JI, Estévez F, Quintana J & Bermejo J, Steroidal saponins from the bark of Dracaena draco and their cytotoxic activities. *J Nat Prod*, 66 (2003) 793.

9 Chen B, McConnell KJ, Wale N, Wild DJ & Gifford EM, Comparing bioassay response and similarity ensemble approaches to probing protein pharmacology. *Bioinformatics*, 27 (2011) 3044.

10 Szklarczyk D, Gable AL, Nastou KC, Lyon D, Kirsch R, Pyysalo S, Doncheva NT, Legeay M, Fang T, Bork P, Jensen LJ & von Mering C, The STRING database in 2021:

customizable protein-protein networks, and functional characterization of user-uploaded gene/measurement sets. *Nucleic Acids Res*, 49 (2021) D605.
11 Clarke DJB, Kuleshov MV, Schilder BM, Torre D, Duffy ME, Keenan AB, Lachmann A, Feldmann AS, Gundersen GW, Silverstein MC, Wang Z & Ma'ayan A, eXpression2Kinases (X2K) Web: linking expression signatures to upstream cell signaling networks. *Nucleic Acids Res*, 46 (2018) W171.
12 Hoang CV, Tu TQ, Nguyen HD & Chu MH, In silico studies of saponins from Hoya verticillata var. verticillate with important apoptosis potency. *Lett Org Chem*, 22 (2025) 846.
13 Casara P, Davidson J, Claperon A, Toumelin-Braizat GL, Vogler M, Bruno A, Chanrion M, Lysiak-Auvity G, Le Diguarher T, Starck JB & Chen I, S55746 is a novel orally active BCL-2 selective and potent inhibitor that impairs hematological tumor growth. *Oncotarget*, 9 (2018) 20075.
14 Van Der Spoel D, Lindahl E, Hess B, Groenhof G, Mark AE & Berendsen HJC, GROMACS: Fast, flexible, and free. *J Comput Chem*, 26 (2005) 1701.
15 Guex N & Peitsch MC, SWISS-MODEL and the Swiss-Pdb Viewer: An environment for comparative protein modeling. *Electrophoresis*, 18 (1997) 2714.
16 Zoete V, Cuendet MA, Grosdidier A & Michielin O, SwissParam: A fast force field generation tool for small organic molecules. *J Comput Chem*, 32 (2011) 2359.
17 Pettersen EF, Goddard TD, Huang CC, Couch GS, Greenblatt DM, Meng EC & Ferrin TE, UCSF Chimera-A visualization system for exploratory research and analysis. *J Comput Chem*, 25 (2004) 1605.
18 Pires DEV, Blundell TL & Ascher DB, pkCSM: Predicting small-molecule pharmacokinetic and toxicity properties using graph-based signatures. *J Med Chem*, 58 (2015) 4066.
19 Neese F, Software Update: The ORCA program system-version 6.0. *WIREs Comput Mol Sci*, 15 (2025) e70019.
20 Hanwell MD, Curtis DE, Lonie DC, Vandermeersch T, Zurek E & Hutchison GR, Avogadro: an advanced semantic chemical editor, visualization, and analysis platform. *J Cheminform*, 4 (2012) 17.
21 Knizia G & Klein JEMN, Electron flow in reaction mechanisms-revealed from first principles. *Angew Chemie Int Ed*, 54 (2015) 5518.
22 Luo J, Xue ZQ, Liu WM, Wu JL & Yang ZQ, Koopmans' Theorem for large molecular systems within density functional theory. *J Phys Chem A*, 110 (2006) 12005.
23 Nguyen CH, Schlerka A, Grandits AM, Koller E, van der Kouwe E, Vassiliou GS, Staber PB, Heller G & Wieser R, IL2RA promotes aggressiveness and stem cell-related properties of acute myeloid leukemia. *Cancer Res*, 80 (2020) 4527.
24 Sahores A, González AR, Yaneff A, May M, Gómez N, Monczor F, Fernández N, Davio C & Shayo C, Ceefourin-1, a MRP4/ABCC4 inhibitor, induces apoptosis in AML cells enhanced by histamine. *Biochim Biophys Acta - Gen Subj*, 1867 (2023) 130322.
25 Wei Y, Cao Y, Sun R, Cheng L, Xiong X, Jin X, He X, Lu W & Zhao M, Targeting Bcl-2 proteins in acute myeloid leukemia. *Front Oncol*, 10 (2020) 584974.
26 Kaloni D, Diepstraten ST, Strasser A & Kelly GL, BCL-2 protein family: attractive targets for cancer therapy. *Apoptosis*, 28 (2023) 20.
27 Duan L, Dong S, Huang K, Cong Y, Luo S & Zhang JZH, Computational analysis of binding free energies, hotspots and the binding mechanism of Bcl-xL/Bcl-2 binding to Bad/Bax. *Phys Chem Chem Phys*, 23 (2021) 2025.
28 Tarakeshwar P, Kim D, Lee HM, Sun SB & Kim KS, Theoretical Approaches to the Design of Functional Nanomaterials, in *Computational Materials Science* (Elsevier, Amsterdam) 2004, 119.
29 Sun Q, The hydrophobic effects: Our current understanding. *Molecules*, 27 (2022) 7009.
30 Harren T, Gutermuth T, Grebner C, Hessler G & Rarey M, Modern machine-learning for binding affinity estimation of protein-ligand complexes: Progress, opportunities, and challenges. *WIREs Comput Mol Sci*, 14 (2024) e1716.
31 Valentini E, D'Aguanno S, Di Martile M, Montesano C, Ferraresi V, Patsilinakos A, Sabatino M, Antonini L, Chiacchiarini M, Valente S, Mai A, Colotti G, Ragno R, Trisciuoglio D & Del Bufalo D, Targeting the anti-apoptotic Bcl-2 family proteins: machine learning virtual screening and biological evaluation of new small molecules, *Theranostics*, 12 (2022) 2427.
32 Ramos J, Muthukumaran J, Freire F, Paquete-Ferreira J, Otrelo-Cardoso AR, Svergun D, Panjkovich A & Santos-Silva T, Shedding light on the interaction of human anti-apoptotic Bcl-2 protein with ligands through biophysical and *in silico* studies, *Int J Mol Sci*, 20 (2019) 860.
33 Rahimi M, Taghdir M & Abasi Joozdani F, Dynamozones are the most obvious sign of the evolution of conformational dynamics in HIV-1 protease. *Sci Rep*, 13 (2023) 14179.
34 Herschlag D & Pinney MM, Hydrogen Bonds: Simple after all? *Biochemistry*, 57 (2018) 3338.
35 Rahman MM, Saha T, Islam KJ, Suman RH, Biswas S, Rahat EU, Hossen MR, Islam R, Hossain MN, Mamun AAl, Khan M, Ali MA & Halim MA, Virtual screening, molecular dynamics and structure-activity relationship studies to identify potent approved drugs for Covid-19 treatment. *J Biomol Struct Dyn*, 39 (2021) 6231.
36 Aghajanpour S, Amiriara H, Esfandyari-Manesh M, Ebrahimnejad P, Jeelani H, Henschel A, Singh H, Dinarvand R & Hassan S, Utilizing machine learning for predicting drug release from polymeric drug delivery systems. *Comput Biol Med*, 188 (2025) 109756.
37 Suenderhauf C, Hammann F & Huwyler J, Computational prediction of blood-brain barrier permeability using decision tree induction. *Molecules*, 17 (2012) 10429.
38 Ramasamy S, Kiew LV & Chung LY, Inhibition of human cytochrome P450 enzymes by bacopa monnieri standardized extract and constituents. *Molecules*, 19 (2014) 2588.
39 Sabe VT, Ntombela T, Jhamba LA, Maguire GEM, Govender T, Naicker T & Kruger HG, Current trends in computer aided drug design and a highlight of drugs discovered via computational techniques: A review. *Eur J Med Chem*, 224 (2021) 113705.
40 Paneru TR, Chaudhary MK, Tandon P, Chaudhary T & Joshi BD, Theoretical study on molecular stability, reactivity, and drug potential of cirsilineol from DFT and molecular docking methods. *Chem Phys Impact*, 8 (2024) 100641.
41 Adindu EA, Godfrey OC, Agwupuye EI, Ekpong BO, Agurokpon DC, Ogbodo SE, Benjamin I & Louis H, Structural analysis, reactivity descriptors (HOMO-LUMO,

ELF, NBO), effect of polar (DMSO, EtOH, H2O) solvation, and libido-enhancing potential of resveratrol by molecular docking. *Chem Phys Impact*, 7 (2023) 100296.

42 Kaya S & Kaya C, A new method for calculation of molecular hardness: A theoretical study. *Comput Theor Chem*, 1060 (2015) 66.

43 Dong X, Oganov AR, Cui H, Zhou XF & Wang HT, Electronegativity and chemical hardness of elements under pressure. *Proc Natl Acad Sci*, 119 (2022) e2117416119.

44 Azeez YH, Kareem RO, Qader AF, Omer RA & Ahmed LO, Spectroscopic characteristics, stability, reactivity, and corrosion inhibition of AHPE-dop compounds incorporating (B, Fe, Ga, Ti): a DFT investigation. *Next Mater*, 3 (2024) 100184.

45 Wei H, Wang H, Wang G, Qu L, Jiang L, Dai S, Chen X, Zhang Y, Chen Z, Li Y, Guo M & Chen Y, Structures of p53/BCL-2 complex suggest a mechanism for p53 to antagonize BCL-2 activity, *Nat Commun*, 14 (2023) 4300.